Model-based Voltage Phase Control for IPMSM with Equilibrium Point Search

Takayuki Miyajima[1], Hiroshi Fujimoto[1], Masami Fujitsuna[2]
[1]The University of Tokyo, [2]DENSO CORPORATION
[1]5-1-5 Kashiwanoha, Kashiwa, Chiba, Japan, [2]1-1 Syouwacho, Kariya, Aichi, Japan
Tel.: [1]+81 / (4) 7136.3881., [2]+81 / (566) 25.6992.
Fax: [1]+81 / (4) 7136.3881., [2]+81 / (566) 25.4552.
Email: miya@fujilab.k.u-tokyo.ac.jp, fujimoto@k.u-tokyo.ac.jp,
MASAMI_FUJITSUNA@denso.co.jp

Keywords

<<Electrical drive>>, <<Permanent magnet motor>>, <<High speed drive>>

Abstract

This paper presents a model-based design method of voltage phase controller for IPMSM with equilibrium point search. The voltage phase controller controls the torque with the output voltage phase only in high-speed region where the inverter output voltage amplitude is saturated. However, voltage phase control cannot achieve quick torque response because it is designed in defiance of transient characteristic. Due to the nonlinear characteristic between torque and voltage phase, precise model-based design have not yet been carried out. In this paper, a model-based design is proposed by the linearizing the relationship between torque and voltage phase. The analysis of the proposed model describes that the plant is a non-minimum phase system. Simulation results and experimental results show the effectiveness of the model-based design method.

Introduction

IPMSMs (Interior Permanent Magnet Synchronous Motors) have been employed in driven systems of electric vehicles, hybrid electric vehicles, and railway vehicles owing to high efficiency and high power density. In order to reduce the size and improve the efficiency of IPMSM, high speed operation is desirable. However, in electric and hybrid electric vehicles, dc-bus voltage is limited by the volume of the installed battery pack. Increment of the battery pack is not preferred considering its cost and vehicle mass.

The fundamental components of the inverter output voltage can be increased by utilizing overmodulation range [1]. Furthermore, flux-weakening control can expand the operating range of IPMSM. In order to minimize copper loss, it is preferred to apply flux-weakening control under maximum output voltage. Also quick torque response is a significant issue which can be greatly contributed to electric vehicle motion control methods [2]. However, due to the inverter output voltage saturation, quick torque response cannot be expected in flux-weakening region. This deteriorates vehicle motion control and vehicle stability. Therefore, quicker torque control technique under voltage amplitude saturation is essential.

In order to achieve quick torque response, feedforward control approaches have been proposed. The model-predictive control [3–5] determines control input which optimizes the defined cost function such as torque tracking error. It can easily consider the voltage limit. The authors proposed 2-DOF control methods based on the perfect tracking control [6] and the final-state control [7]. Since feedforward control cannot suppress parameter variation, robust feedback control method is necessary. The voltage limiter methods [8, 9] operate current controller output so as to quicken its response. During this operation, the current feedback loop becomes an open-loop and stability is not guaranteed. The modulation index feedback methods [10–12] modified d-axis current reference. However, modulation feedback

method cannot achieve quick torque response because the modulation feedback loop is the outer of the current feedback loop which has low bandwidth due to voltage saturation.

During flux-weakening control, the voltage amplitude is fixed and the control input is the voltage phase only. The voltage phase control [13, 14] operates voltage phase directly to compensate torque tracking error. However, the controller gains are determined by trial and error because of its nonlinear characteristics. [15] proposed a model-based design using linerized IPMSM model under small voltage phase. Thus, it cannot consider IPMSM characteristic precisely when the voltage phase is large. In induction motors, transfer function between voltage phase and q-axis current had been analyzed [16, 17]. However it focused only on resonance peak of linearized transfer function in order to design the torque reference filter of modulation feedback system. Thus, the transient characteristic between torque and voltage phase has not been discussed precisely. This paper investigates the relationship between torque and the voltage angle and focuses on voltage phase controller design for IPMSM.

For preise model-based design, this paper presents the transfer function between torque and voltage phase by using linearization. An analysis of the proposed plant model shows that the plant is a non-minimum phase system depending on operating point. A non-minimum phase system is the system whose zero is unstable [18]. Feedback control systems of a non-minimum phase system have the trade-off between undershoot and settling time. This trade-off is an achievable performance limitation of voltage phase control. The proposed design method selects a PID controller as voltage phase controller in order to place all closed-loop poles to arbitrary values though these poles are slower than a zero of the plant to avoid undershoot. Simulation results and experimental results in the linear range of an inverter show the effectiveness of the proposed design method. Finally, experimental result verifies that it can be applied to six-step operation.

Model and linearization

IPMSM model

The voltage equations of IPMSM are represented by

$$\dot{\boldsymbol{x}}(t) = \boldsymbol{f}(\boldsymbol{x},\ \boldsymbol{u}) = \begin{bmatrix} -\frac{R}{L_q} & \omega_e \frac{L_q}{L_d} \\ -\omega_e \frac{L_d}{L_q} & -\frac{R}{L_q} \end{bmatrix} \boldsymbol{x}(t) + \begin{bmatrix} \frac{v_d(\boldsymbol{u})}{L_d} \\ \frac{v_q(\boldsymbol{u}) - \omega_e K_e}{L_q} \end{bmatrix}, \tag{1}$$

$$v_d(\boldsymbol{u}) = -V_a(t)\sin\delta(t), \quad v_q(\boldsymbol{u}) = V_a(t)\cos\delta(t), \tag{2}$$

$$\boldsymbol{x}(t) := [i_d(t) \quad i_q(t)]^{\mathrm{T}}, \quad \boldsymbol{u}(t) := [V_a(t) \quad \delta(t)]^{\mathrm{T}}, \tag{3}$$

where v_d, v_q, i_d, i_q, L_d, and L_q are the d- and q-axis voltages, currents, and inductances, R is the stator winding resistance, ω_e is the electric angular velocity, K_e is the back EMF constant, V_a is the voltage amplitude, and δ is the voltage phase.

The torque T is described as

$$T(t) = K_{mt} i_q(t) + K_{rt} i_d(t) i_q(t), \tag{4}$$

where $K_{mt} := PK_e$, $K_{rt} := P(L_d - L_q)$, and P is the number of pole pairs. Under the voltage amplitude saturation, the control variable is the voltage phase only. From (1), (2), and (4), the relationship between the torque and the voltage phase is nonlinear. Therefore, for model-based design, the authors derive the linear transfer function with linearization.

Linearization

The model-based design of the voltage phase controller is difficult because the relationship between torque and voltage phase is nonlinear. Therefore, for model-based design, a linear plant model is derived by linearization.

At first, the voltage equation (1) is linearized. Consider the equilibrium point $(\boldsymbol{x}_o,\ \boldsymbol{u}_o)$ which satisfies $\boldsymbol{f}(\boldsymbol{x}_o,\ \boldsymbol{u}_o) = \boldsymbol{0}$, where $\boldsymbol{u}_o = [V_{ao} \quad \delta_o]^{\mathrm{T}}$ and $\boldsymbol{x}_o = [i_{do} \quad i_{qo}]^{\mathrm{T}}$. (1) can be linearized around this

equilibrium point by using first-order Taylor series as follows:

$$\frac{\mathrm{d}}{\mathrm{d}t}\begin{bmatrix}\Delta i_d(t)\\ \Delta i_q(t)\end{bmatrix} = \boldsymbol{A}\begin{bmatrix}\Delta i_d(t)\\ \Delta i_q(t)\end{bmatrix} + \boldsymbol{B}\begin{bmatrix}\Delta V_a(t)\\ \Delta\delta(t)\end{bmatrix}, \tag{5}$$

$$\boldsymbol{A} := \left.\frac{\partial \boldsymbol{f}}{\partial \boldsymbol{x}}\right|_{(\boldsymbol{x}_o,\boldsymbol{u}_o)} = \begin{bmatrix}-\frac{R}{L_d} & \omega_e\frac{L_q}{L_d}\\ -\omega_e\frac{L_d}{L_q} & -\frac{R}{L_q}\end{bmatrix}, \tag{6}$$

$$\boldsymbol{B} := \left.\frac{\partial \boldsymbol{f}}{\partial \boldsymbol{u}}\right|_{(\boldsymbol{x}_o,\boldsymbol{u}_o)} = \begin{bmatrix}-\frac{1}{L_d}\sin\delta_o & -\frac{V_{ao}}{L_d}\cos\delta_o\\ \frac{1}{L_q}\cos\delta_o & -\frac{V_{ao}}{L_q}\sin\delta_o\end{bmatrix}, \tag{7}$$

$$\Delta i_d := i_d - i_{do}, \quad \Delta i_q := i_q - i_{qo}, \quad \Delta V_a := V_a - V_{ao}, \quad \Delta\delta := \delta - \delta_o.$$

The transfer functions from the voltage amplitude and the voltage phase to the d- and q-axis currents are obtained by

$$\begin{bmatrix}\Delta i_d(s)\\ \Delta i_q(s)\end{bmatrix} = \begin{bmatrix}\Delta P_{11}(s) & \Delta P_{12}(s)\\ \Delta P_{21}(s) & \Delta P_{22}(s)\end{bmatrix}\begin{bmatrix}\Delta V_a(s)\\ \Delta\delta(s)\end{bmatrix}, \tag{8}$$

$$\Delta P_{11}(s) = \frac{-\frac{1}{L_d}\sin\delta_o\left\{s + \frac{R}{L_q} - \omega_e\tan\left(\frac{\pi}{2} - \delta_o\right)\right\}}{s^2 + a_1 s + a_0}, \tag{9}$$

$$\Delta P_{12}(s) = \frac{-\frac{V_{ao}}{L_d}\cos\delta_o\left(s + \frac{R}{L_q} + \omega_e\tan\delta_o\right)}{s^2 + a_1 s + a_0}, \tag{10}$$

$$\Delta P_{21}(s) = \frac{\frac{1}{L_q}\cos\delta_o\left(s + \frac{R}{L_d} + \omega_e\tan\delta_o\right)}{s^2 + a_1 s + a_0}, \tag{11}$$

$$\Delta P_{22}(s) = \frac{-\frac{V_{ao}}{L_q}\sin\delta_o\left\{s + \frac{R}{L_d} - \omega_e\tan\left(\frac{\pi}{2} - \delta_o\right)\right\}}{s^2 + a_1 s + a_0}. \tag{12}$$

$$a_1 := \frac{R}{L_d} + \frac{R}{L_q},\ a_0 := \frac{R^2}{L_d L_q} + \omega_e^2$$

Secondly, the torque (4) is approximated to a linear function as follow:

$$\begin{aligned} T &= T_o + \Delta T = K_{mt}(i_{qo} + \Delta i_q) + K_{rt}(i_{do} + \Delta i_d)(i_{qo} + \Delta i_q),\\ \Delta T &= K_{mt}\Delta i_q + K_{rt}(\Delta i_d i_{qo} + i_{do}\Delta i_q + \Delta i_d\Delta i_d), \end{aligned} \tag{13}$$

where T_o is the torque at equilibrium point. Here, it is assumed that $\Delta i_d \Delta i_d$ can be neglected. (13) can be approximated as

$$\Delta T \simeq (K_{mt} + K_{rt} i_{do}) \cdot \Delta i_q + K_{rt} i_{qo} \cdot \Delta i_d. \tag{14}$$

Finally, the linear transfer function is derived. By substituting (9)-(12) into (14), the transfer functions from the voltage amplitude and the voltage phase to the torque are given by

$$\Delta T(s) = [\Delta P_{T1}(s) \quad \Delta P_{T2}(s)] \cdot \begin{bmatrix}\Delta V_a(s)\\ \Delta\delta(s)\end{bmatrix}, \tag{15}$$

$$\Delta P_{T1}(s) = \frac{b_{T11}s + b_{T10}}{s^2 + a_1 s + a_0}, \tag{16}$$

$$\Delta P_{T2}(s) = \frac{b_{T21}s + b_{T20}}{s^2 + a_1 s + a_0}, \tag{17}$$

$$b_{T11} := \sqrt{\frac{K_1^2}{L_q^2} + \frac{K_2^2}{L_d^2}}\cos\left(\delta_o + \tan^{-1}\frac{K_2 L_q}{K_1 L_d}\right),$$

Table I: nominal parameters under the test

stator winding resistance R	140.2 mΩ	P	3
d-axis inductance L_d	0.516 mH	dc-bus voltage V_{dc}	36.0 V
q-axis inductance L_q	1.61 mH	maximum modulation index $M_{\max}$	1.15
back EMF constant K_e	42.55 mV/(rad/s)	base speed	1000 rpm

$$
\begin{aligned}
b_{T10} :=& \frac{R}{L_d L_q}\sqrt{K_1^2+K_2^2}\cos\left(\delta_o+\tan^{-1}\frac{K_2}{K_1}\right)+\omega_e\sqrt{\frac{K_1^2}{L_q^2}+\frac{K_2^2}{L_d^2}}\sin\left(\delta_o+\tan^{-1}\frac{K_2L_q}{K_1L_d}\right),\\
b_{T21} :=& -V_{ao}\sqrt{\frac{K_1^2}{L_q^2}+\frac{K_2^2}{L_d^2}}\sin\left(\delta_o+\tan^{-1}\frac{K_2L_q}{K_1L_d}\right),\\
b_{T20} :=& -V_{ao}\frac{R}{L_dL_q}\sqrt{K_1^2+K_2^2}\sin\left(\delta_o+\tan^{-1}\frac{K_2}{K_1}\right)\\
&+V_{ao}\omega_e\sqrt{\frac{K_1^2}{L_q^2}+\frac{K_2^2}{L_d^2}}\cos\left(\delta_o+\tan^{-1}\frac{K_2L_q}{K_1L_d}\right),\\
K_1 :=& K_{mt}+K_{rt}i_{do},\ K_2 := K_{rt}i_{qo}.
\end{aligned}
$$

The proposed voltage phase controller design method uses the linearized plant model $\Delta P_{T2}(s)$.

Analysis of linearized plant model

From the viewpoint of zeros, the characteristics of the transfer functions from voltage phase to d- and q-axis currents and torque are studied. The zeros are the roots of the transfer function numerator polynomial. The zeros of $\Delta P_{12}(s)$ and $\Delta P_{22}(s)$ are represented by (18) and (19), respectively.

$$z_{12} = -\frac{R}{L_q} - \omega_e \tan\delta_o. \tag{18}$$

$$z_{22} = -\frac{R}{L_d} + \omega_e \tan\left(\frac{\pi}{2}-\delta_o\right). \tag{19}$$

The voltage phase control operates within monotone increasing range between torque and voltage phase. If the stator winding resistance R can be neglected, the average torque $\bar{T}$ is represented by

$$\bar{T} = \frac{K_{mt}V_a}{\omega_e L_d}\sin\delta + \frac{V_a^2}{2\omega_e^2}\left(\frac{1}{L_q}-\frac{1}{L_d}\right)\sin 2\delta. \tag{20}$$

From this equation, the monotone increasing range is $[-\pi/2\ \pi/2]$. In the flux-weakening region, $\frac{R}{L_d} \ll \omega_e$ and $\frac{R}{L_q} \ll \omega_e$. Therefore, during motoring mode ($0 < \delta_o < \pi/2$), $\Delta P_{12}(s)$ and $\Delta P_{22}(s)$ have a stable zero and an unstable zero, respectively. On the other hand, under regeneration ($-\pi/2 < \delta_o < 0$), $\Delta P_{12}(s)$ and $\Delta P_{22}(s)$ have an unstable zero and a stable zero, respectively.

Here, the unstable zero is the zero which lies in right-half plane. If the unstable zero is slow, it obtains large undershoot. The stable zero is the zero which lies in left-half plane. Large overshoot is given when the stable zero is slow.

The property between the voltage phase and the torque is determined by the combination with these characteristics. A zero of $\Delta P_{T2}(s)$ is expressed by $-b_{T20}/b_{T21}$. However, it is a complex nonlinear function of the operation point. Thus, the value of the zero is given by numerical calculation. The result is shown in Fig. 1. Here, Table I illustrates the nominal parameters of the test.

As shown in Fig. 1, the value of the zero depends on the operation point. Fig. 1(b) demonstrates that the plant has a slow unstable zero at high-speed and high-torque region. On the other hand, during regeneration at high-speed and high-torque region, the plant has a stable zero.

The above analysis means that the voltage phase controller has a trade-off between quick torque response and small undershoot in high-speed and high-torque region.

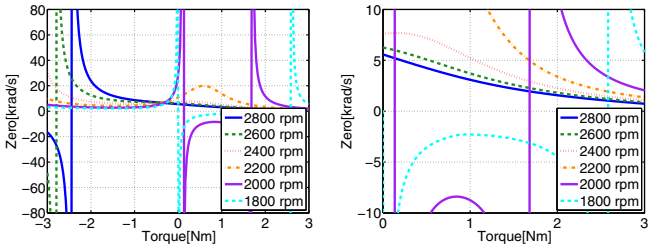

(a) the value of a zero (b) the value of a zero (zoom)

Fig. 1: A zero of ΔP_{T2} under maximum modulation index.

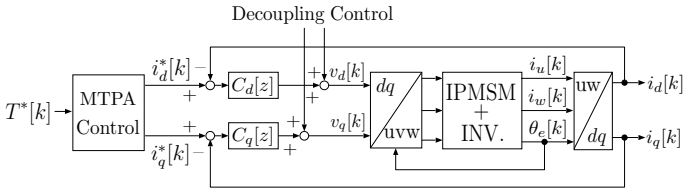

Fig. 2: Block diagram of the current vector control.

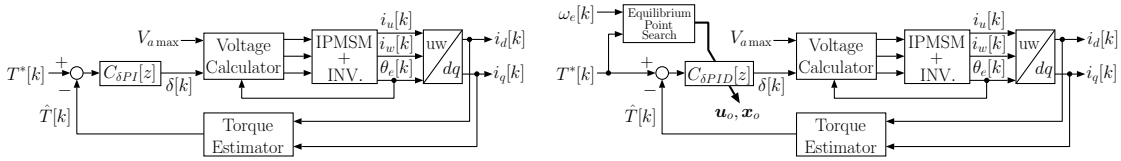

(a) conventional method (b) proposed method

Fig. 3: Block diagram of the voltage phase control.

Control system design

In this paper, the control system consists of three components: the current vector control shown in Fig. 2, the voltage phase control described in Fig. 3, and the control switch structure. If the voltage amplitude is not saturated, the current vector control is applied to the control system. At the operating point on the voltage limit ellipse, the torque is controlled with the voltage phase controller.

The conventional method uses a voltage phase PI controller which is determined by trial and error. On the other hand, the voltage phase controller of the proposed method is a PID controller which is designed based on the precise plant model $\Delta P_{T2}(s)$. Briefly, the difference between the conventional method and the proposed method is the design of voltage phase controller only.

Current vector control

"MTPA control" in Fig. 2 generates the d- and q-axis current references from the torque reference T^* based on the maximum torque per ampere (MTPA) control by using look-up table. The coupling terms in (1) are rejected by the decoupling controls which are represented by

$$v_d[k] = v'_d[k] - \omega_e[k] L_q i_q[k], \tag{21}$$

$$v_q[k] = v'_q[k] + \omega_e[k](L_d i_d[k] + K_e), \tag{22}$$

where v'_d and v'_q denote the d- and q- axis current feedback controller outputs, respectively.

The d- and q-axis current feedback controllers are designed to be a plant-pole cancellation feedback control as follow:

$$C_d(s) = \frac{L_d s + R}{\tau s}, \quad C_q(s) = \frac{L_q s + R}{\tau s}, \quad \tau = 1.0 \text{ ms}, \tag{23}$$

where τ is the selected bandwidth of the current loop. The discretized controllers $C_d[z]$ and $C_q[z]$ by the Tustin transform are applied to the control system.

When the voltage reference is saturated before switching to the voltage phase control, it is limited as

$$\tilde{\boldsymbol{V}}_a[k] = \begin{cases} \frac{\boldsymbol{V}_a[k]}{|\boldsymbol{V}_a[k]|} V_{a\max} & (|\boldsymbol{V}_a[k]| > V_{a\max}) \\ \boldsymbol{V}_a[k] & (\text{otherwise}) \end{cases}, \tag{24}$$

where $\boldsymbol{V}_a = [v_d \quad v_q]^{\mathrm{T}}$, $\tilde{\boldsymbol{V}}_a$ is the limited voltage reference, and $V_{a\max}(:= \sqrt{3/2} M_{\max} V_{dc})$ is the maximum voltage amplitude. Here, $\sqrt{3/2}$ is the coefficient to transform two-phase into three-phase. Under voltage amplitude saturation, an anti-windup control in [19] is applied.

Conventional voltage phase control [13]

The conventional voltage phase controller reported in Fig. 3(a) uses a PI controller which is expressed as

$$C_{\delta PI}(s) = \frac{K_P s + K_I}{s}, \tag{25}$$

where K_I and K_P are the integral and proportional gains. These gains are determined by trial and error. By discretizing with Tustin transform, $C_{\delta PI}[z]$ is obtained. Then, $\hat{T}$ is calculated from (5) using nominal parameters.

During the voltage phase control, constant voltage amplitude $V_{a\max}$ is given.

Proposed voltage phase control

The voltage phase controller of the proposed method is designed with the precise plant model $\Delta P_{T2}(s)$. However, this model is derived around an equilibrium point. The voltage phase controller is used during the voltage amplitude saturation. Thus, the equilibrium point is an intersection of the voltage limit ellipse and the torque constant curve. Although this intersection cannot be easily derived because of high order polynomial equation, it can be calculated with the Newton-Raphson method. This algorithm can be represented by

$$\boldsymbol{x}_{o,\,k+1} = \boldsymbol{x}_{o,\,k} + \boldsymbol{\Psi}^{-1}(\boldsymbol{x}_{o,\,k}) \cdot \boldsymbol{\psi}(\boldsymbol{x}_{o,\,k}), \tag{26}$$

$$\boldsymbol{\psi}(\boldsymbol{x}_o) := \begin{bmatrix} g(\boldsymbol{x}_o) \\ h(\boldsymbol{x}_o) \end{bmatrix}, \quad \boldsymbol{\Psi}(\boldsymbol{x}_o) := \frac{\partial \boldsymbol{\psi}(\boldsymbol{x}_o)}{\partial \boldsymbol{x}_o}^{\mathrm{T}},$$

$$g(\boldsymbol{x}_o) = V_{a\max}^2 - \{R i_{qo} + \omega_e (L_d i_{do} + K_e)\}^2 - (R i_{do} - \omega_e L_q i_{qo})^2 = 0, \tag{27}$$

$$h(\boldsymbol{x}_o) = T^* - K_{mt} i_{qo} - K_{rt} i_{do} i_{qo} = 0, \tag{28}$$

where $\boldsymbol{x}_{o,\,k}$ denotes the solution after k-th time iterating, $g(\boldsymbol{x}_o)$ means the voltage limit ellipse, and $h(\boldsymbol{x}_o)$ is the constant torque curve which satisfies torque reference. This scheme calculates (26) once during one sampling time and stops the iteration when $|\boldsymbol{\Psi}(\boldsymbol{x}_{o,\,k})| \simeq 0$. If $i_{do,\,k+1} > 0$, the scheme limited as $i_{do,\,k+1} = 0$. Here, the initial value $\boldsymbol{x}_{o,\,0}$ is given from the current references during the current vector control. $\boldsymbol{u}_o$ is also determined by $\boldsymbol{f}(\boldsymbol{x}_o,\ \boldsymbol{u}_o) = 0$.

In the proposed design method, in order to place all closed-loop poles to arbitrary values, a PID controller is selected as the voltage phase controller. The PID controller $C_{\delta PID}(s)$ is designed by pole placement using the plant model $\Delta P_{T2}(s)$ which is around the calculated equilibrium point. The parameters of $\Delta P_{T2}(s)$ vary depending on the operating point, namely, the proposed voltage phase controller is a variable gain controller.

Controller switch structure

The switching condition from the current vector control to the voltage phase control is based on torque tracking error. If this torque response $\hat{T}$ takes longer than intended torque response T_n^*, the controller switch structure switches to the voltage phase control. (29) describes the sum of the difference e_{Tn} between T_n^* and $\hat{T}$. Here, $e_T(:= T^* - \hat{T}[k])$ is the torque tracking error.

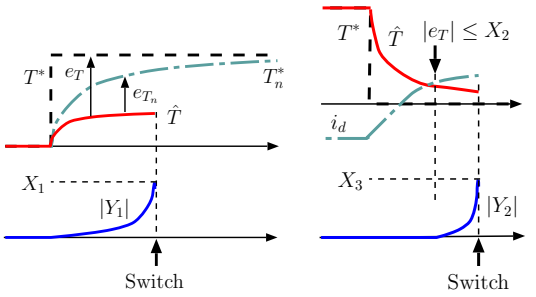

(a) Switch to voltage phase control (b) Switch to current vector control

Fig. 4: Switching condition.

$$Y_1[k] = \begin{cases} e_{T_n} + Y_1[k-1] & (V_a \geq V_{a\max} \ \& \ \mathrm{sgn}(e_T)e_{T_n} > 0) \\ 0 & (\text{otherwise}) \end{cases}. \tag{29}$$

As shown in Fig. 4(a), right after Y_1 exceeds the baseline X_1, the voltage phase controller starts to work. After switching to the voltage phase control, in order to suppress the discontinuity of control input, the voltage phase at the last sampling time of the current vector control is given as feedforward input.

On the other hand, the switching condition from the voltage phase control to the current vector control is based on the value of d-axis current. The intersection of the constant torque curve and MTPA curve exists inside voltage limit ellipse, if $i_d^* - i_d > 0$ where i_d^* is the d-axis current reference under the current vector control. It means that the torque reference can be achieved by the current vector control. Therefore, the control system is switched to the current vector control. (30) expresses the sum of the d-axis current error $e_d (:= i_d^* - i_d)$ under smaller torque tracking error than X_2.

$$Y_2[k] = \begin{cases} e_d + Y_2[k-1] & (|e_T| \leq X_2 \ \& \ e_d < 0) \\ 0 & (\text{otherwise}) \end{cases}. \tag{30}$$

If Y_2 is smaller than the baseline X_3, the voltage phase controller is applied to the control system. At this point, in order to prevent discontinuity of control inputs, the initial state variables of the current feedback controllers are compensated from the voltage phase controller output as follows:

$$x_{fbd}[k+1] = -V_{a\max} \sin\delta[k] + \omega_e L_q i_q - D_{fbd} e_d[k] + B_{fbd} e_d[k], \tag{31}$$

$$x_{fbq}[k+1] = V_{a\max} \cos\delta[k] - \omega_e (L_d i_d + K_e) - D_{fbq} e_q[k] + B_{fbq} e_q[k], \tag{32}$$

where B_{fbd}, B_{fbq}, D_{fbd}, and D_{fbq} are B and D matricies of d-axis and q-axis current FB controllers, x_{fbd}, x_{fbq} are state variables of FB controllers, e_{id}, e_{iq} are d-axis and q-axis current errors between current and current reference of MPTA control.

In this paper, X_1, X_2, and X_3 are determined by trial and error. Both the conventional method and the proposed method use the same control switch structure.

Simulation

The proposed design method is evaluated firstly by simulation results. The parameters under simulations are the same as Table I. The sampling period is 0.1 ms. The parameters of the control switch structure are as follows: $X_1 = 40$, $X_2 = 0.1$, $X_3 = -80$, and the torque reference that goes through low-pass filter whose time constant is 5.0 ms is given as the desired torque response T_n^*.

The gains of the conventional voltage phase controller are determined by trial and error so that the transient response becomes small damped oscillation. The control gains are $K_P = 0.001$ and $K_I = 30$.

The plant poles are expressed by

$$p_1,\ p_2 = -\frac{R}{2}\left(\frac{1}{L_d} + \frac{1}{L_q}\right) \pm j\sqrt{\omega_e^2 - \frac{R^2}{4}\left(\frac{1}{L_d} - \frac{1}{L_q}\right)^2}. \tag{33}$$

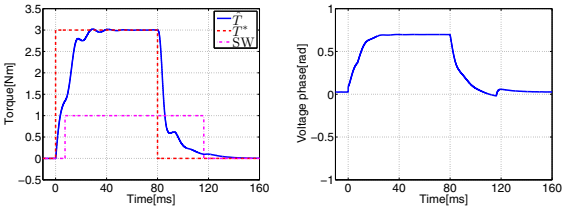

(a) Torque (b) Voltage phase

Fig. 5: Simulation result 1 (1600 rpm, conventional method, linear range).

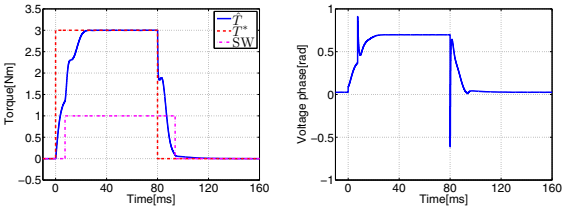

(a) Torque (b) Voltage phase

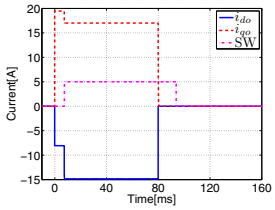

(c) Equilibrium point

Fig. 6: Simulation result 1 (1600 rpm, proposed method, linear range).

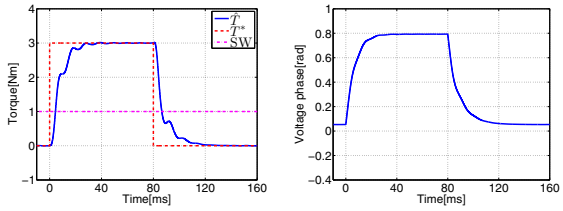

(a) Torque (b) Voltage phase

Fig. 7: Simulation result 2 (2000 rpm, conventional method, linear range).

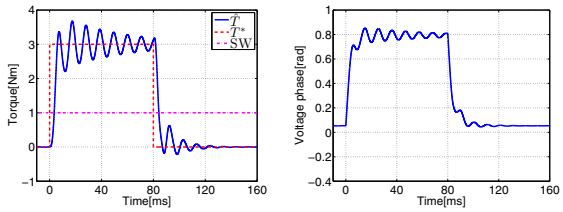

(a) Torque (b) Voltage phase

Fig. 8: Simulation result 2 (2000 rpm, high gain conventional method, $K_I = 55$, linear range).

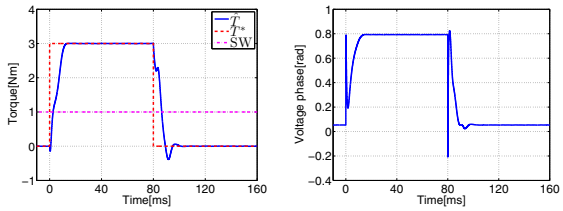

(a) Torque (b) Voltage phase

Fig. 9: Simulation result 2 (2000 rpm, proposed method, linear range).

In high-speed region, the plant has fast complex conjugate poles. All closed-loop poles should be faster than the plant poles. However, fast closed-loop poles cause undershoot because the plant is a non-minimum phase system. Therefore, at the high-speed region, the proposed method places all closed-loop poles on a circle which goes through the plant poles and has a center at the origin. The real parts of two closed-loop poles are set at -550 rad/s and the real part of the others are placed at -350 rad/s.

Fig. 5 and Fig. 6 show step torque responses at 1600 rpm. Here, the "SW" represents the mode of controller. When the SW is "high", the voltage phase control is applied. On the other hand, the current vector control is applied when the SW is "low". In the conventional method, the gains are small. Therefore, the torque response is hardly oscillated but very slow. On the other hand, the proposed method operates voltage phase quickly as shown in Fig. 6(b). Thus, it achieves quick and no oscillation response. Fig. 6(c) shows the equilibrium point search scheme output. After switching to the voltage phase control, the scheme search an equilibrium point at torque reference quickly.

Fig. 7, Fig. 8, and Fig. 9 describe step torque responses at 2000 rpm. According to this simulation, torque is controlled by voltage phase controller only. In Fig. 8, the integral gain is changed to be $K_I = 55$. As a result, torque response is oscillated. In contrast, the proposed method shortens the setting time and oscillation is eliminated. However, overshoot occurs at about 90 ms. The proposed method designs controller around torque reference. Therefore, when step torque reference is obtained, modeling error ours at the beginning of response. This modeling error deteriorates the sensitivity function peak and causes overshoot but quicker torque response is achieved by the proposed method in comparison with the conventional method.

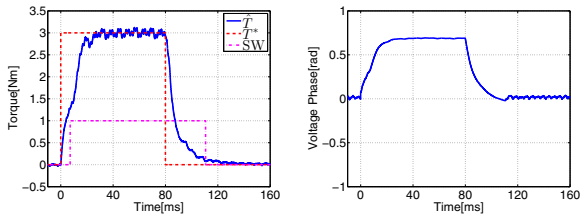

(a) Torque (b) Voltage phase

Fig. 10: Experimental result 1 (1600 rpm, conventional method, linear range).

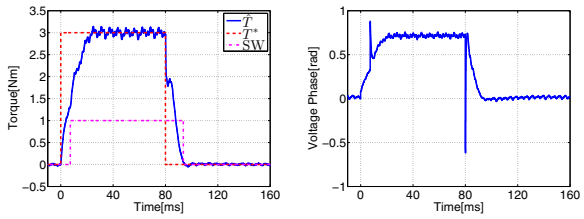

(a) Torque (b) Voltage phase

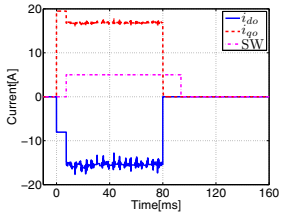

(c) Equilibrium point

Fig. 11: Experimental result 1 (1600 rpm, proposed method, linear range).

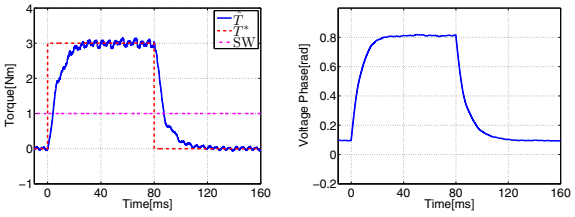

(a) Torque (b) Voltage phase

Fig. 12: Experimental result 2 (2000 rpm, conventional method, linear range).

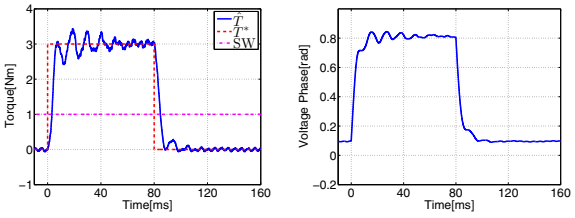

(a) Torque (b) Voltage phase

Fig. 13: Experimental result 2 (2000 rpm, high gain conventional method, $K_I = 55$, linear range).

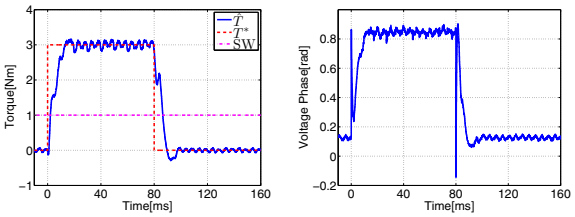

(a) Torque (b) Voltage phase

Fig. 14: Experimental result 2 (2000 rpm, proposed method, linear range).

Experimemnt

Experiments were conducted under the same condition as simulations. A LPF with time constant of 1 ms is utilized to avoid velocity resolution in the proposed voltage phase controller design.

The torque responses of the conventional method and the proposed method are reported in Fig. 10 and Fig. 11, respectively. The speed is 1600 rpm. After switching to the voltage phase control, the proposed method has no oscillation and quick torque response.

The experimental results at 2000 rpm are shown in Fig. 12, Fig. 13 and Fig. 14. Torque response of the conventional method is oscillated by increasing the integral gain. From these results, the problem of the conventional method and the effectiveness of the proposed method are confirmed.

Finally, the experimental results in six-step operation are represented in Fig. 15 and Fig. 16. The proposed design method achieves high performance in both linear range and overmodulation range.

Conclusion

In order to achieve high bandwidth control under voltage saturation, this paper proposes a model-based voltage phase controller design method for IPMSM. Detailed analysis of the proposed precise plant model shows that the relationship between torque and voltage phase is a non-minimum phase system depending on the operating point. In contrast to the conventional method, the proposed method can place arbitrary closed-loop poles by model-based design. The simulation results and experimental results verified the effectiveness of the proposed method in both linear range and six-step operation.

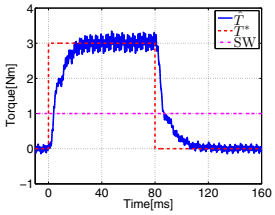

(a) Torque

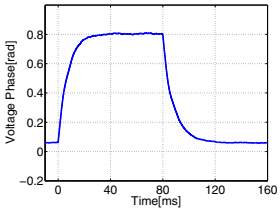

(b) Voltage phase

Fig. 15: Experimental result 3 (2500 rpm, conventional method, six-step operation, $M_{\max} = 1.27$).

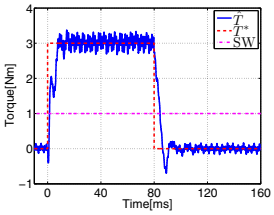

(a) Torque

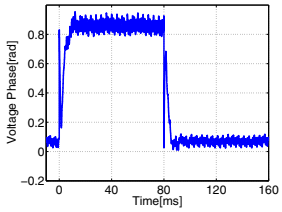

(b) Voltage phase

Fig. 16: Experimental result 3 (2500 rpm, proposed method, six-step operation, $M_{\max} = 1.27$).

References

[1] J. Holtz, W. Lotzkat, and A. M. Khambadkone: "On Continuous Control of PWM Inverters in Overmodulation Range Including the Six-Step Mode", IEEE Trans. Power Electronics, Vol. 8, No. 4, pp. 546–553, 1993.

[2] Y. Hori: "Future Vehicle Driven by Electricity and Control.Research on Four-Wheel-Motored "UOT Electric March II" ", IEEE Trans. Ind. Electron., Vol.51, No.5, pp.954–962, 2004.

[3] T. Geyer: "Computationally Efficient Model Predictive Direct Torque Control", IEEE Trans. Power Electronics, Vol. 26, No. 10, pp. 2804–2816, 2011.

[4] P. Landsmann, and R. Kennel: "Saliency-Based Sensorless Predictive Torque Control With Reduced Torque Ripple", IEEE Trans. Power Electronics, Vol. 27, No. 10, pp. 4311–4320, 2012.

[5] T. Maeda and S. Doki: "Improvement of Torque Control System of PMSM based on Model Predictive Control", 37th Annual Conference on IEEE Industrial Electronics Society, pp. 1891–1896, 2011.

[6] T. Miyajima, H. Fujimoto, and M. Fujitsuna: "Control Method for IPMSM Based on Perfect Tracking Control and PWM Hold Model in Overmodulation Range", The 2010 International Power Electronics Conference, pp.593-598, 2010.

[7] T. Miyajima, H. Fujimoto, and M. Fujitsuna: "Feedforward control for SPMSM with Final State Control Based on Voltage Limit Circle with Transient Term", The 2011 IEEE Energy Conversion Congress and Exposition, pp.3913–3919, 2011.

[8] B.-H. Bae and S.-K. Sul: "A Novel Dynamic Overmodulation Strategy for Fast Torque Control of High-Saliency-Ratio AC Motor", IEEE Trans. Ind. Appl., Vol.41, No.4, pp.1013–1019, 2005.

[9] S. Lerdudomsak, S. Doki, and S. Okuma: "Voltage Limiter Calculation Method for Fast Torque Response of IPMSM in Overmodulation Range", The 35th Annual Conference of the IEEE Industrial Electronics Society, pp. 1385–1390, 2009.

[10] K. Kondo, K. Matsuoka, Y. Nakazawa, and H. Shimizu: "Torque feed-back control for salient pole permanent magnet synchronous motor at weakening flux control range", IEEJ Trans. IA, Vol. 119, No. 10, pp. 1155–1164, 1999 (in Japanese).

[11] T.-S. Kwon, G.-Y. Choi, M.-S. Kwak, and S.-K Sul : "Novel Flux-Weakening Control of an IPMSM for Quasi-Six-Step Operation", IEEE Trans. Ind. Appl., Vol. 44, NO. 6, pp. 1722–1723, 2008.

[12] H. Liu, Z. Q. Zhu, E. Mohamed, Y. Fu, and X. Qi: "Flux-Weakening Control of Nonsalient Pole PMSM Having Large Winding Inductance, Accounting for Resistive Voltage Drop and Inverter Nonlinearities", IEEE Trans. Power Electronics, Vol. 27, No. 2, pp. 942–952, 2012.

[13] H. Nakai, H. Ohtani, E. Satoh, and Y. Inaguma: "Development and Testing of the Torque Control for the Permanent-Magnet Synchronous Motor", IEEE Trans. Ind. Electron., Vol. 52, No. 3, pp. 800–806, 2005.

[14] W. Hatsuse, Y. Notohara, K. Ohi, K. Tobari, K. Tamura, C. Unoko, and Y. Iwaji: "A Stable Field-Weakening Control Using Voltage Phase Operations in the High-Power Region", The 2010 International Power Electronics Conference, pp.599–604, 2010.

[15] K. Kondo and S. Kitamura: "Torque Control Method for Permanent Magnet Synchronous Motor Operating in Field Weakening Region at Middle Speed Range", IEEJ Journal of Industry Applications, Vol. 2, No. 2, pp. 106–112, 2013.

[16] Y. Nakazawa, S. Toda I. Yasuoka, and H. Naito: "One-Pulse PWM Mode Vector Control for Traction Drives", IEEE Power Electronics in Transportation, pp. 135–141, 1996.

[17] Y. Nakazawa, S. Toda, and I. Yasuoka: "A New Vector Control for Induction. Motor Drives in Full Block Mode of Inverters", IEEJ Trans. IA, Vol. 119, No. 9, pp. 1071–1080, 1998 (in Japanese).

[18] J. B. Hag and D. S. Bernstein: "Nonminimum-phase zeros - much to do about nothing - classical control - revisited part II", IEEE Control system magazine, Vol. 27, No. 3, pp. 45–57, 2006.

[19] K. Ohishi, E. Hayasaka, T. Nagano, and H. Masaya: "High-performance speed servo system considering Voltage saturation of a vector-controlled induction motor", IEEE Trans. Ind. Electron., Vol. 5., NO. 3, pp. 795–802, 2006.